

How a stable greenhouse effect on Earth is maintained under global warming

Feng Jing¹, Paynter David², and Menzel Raymond³

¹Princeton University

²GFDL

³UCAR

November 16, 2022

Abstract

Greenhouse gases (GHGs) are gases that absorb and emit thermal energy. In a warming climate, GHGs modulate the thermal cooling to space from the surface and atmosphere, which is a fundamental feedback process that affects climate sensitivity. Previous studies have stated that the thermal cooling to space with global warming is primarily emitted from the surface, rather than the atmosphere. Using a millennium-length coupled general circulation model (Geophysical Fluid Dynamics Laboratory's CM3) and accurate line-by-line radiative transfer calculations, here we show that the atmospheric cooling to space accounts for 12 % to 50 % of Earth's clear-sky longwave feedback parameter from the poles to the tropics. The atmospheric cooling to space is an efficient stabilizing feedback process because water vapor and non-condensable GHGs tend to emit at higher temperatures with surface warming as the thermodynamic structure of the atmosphere evolves. A simple yet comprehensive model is proposed in this study for predicting the clear-sky longwave feedback over a wide range of surface temperatures. It achieves good spectral agreement when compared to line-by-line calculations. Our study provides a theoretical way for assessing Earth's climate sensitivity, with important implications for Earth-like planets.

1 **How a stable greenhouse effect on Earth is maintained**
2 **under global warming**

3 **Jing Feng, David Paynter, Raymond Menzel**

4 ¹Atmospheric and Oceanic Sciences Program, Princeton University, 300 Forrester Road, Princeton,
5 08540-6654, New Jersey, United States

6 ¹Geophysical Fluid Dynamics Laboratory, 201 Forrester Road, Princeton, 08540-6649, New Jersey, United
7 States

8 ¹University Corporation for Atmospheric Research/GFDL, 201 Forrester Road, Princeton, 08540-6649,
9 New Jersey, United States

10 **Key Points:**

- 11 • A long-ignored atmospheric feedback process maintained by greenhouse gases cru-
12 cially stabilizes Earth's climate under global warming.
13 • Earth's clear-sky thermal energy budget is unlikely to runaway due to its stable
14 atmospheric composition and thermodynamic structure.
15 • A simple, analytical model can accurately predict the state-dependent clear-sky
16 longwave feedback spectrum.

Corresponding author: Jing Feng, jing.feng@Princeton.edu

Abstract

Greenhouse gases (GHGs) are gases that absorb and emit thermal energy. In a warming climate, GHGs modulate the thermal cooling to space from the surface and atmosphere, which is a fundamental feedback process that affects climate sensitivity. Previous studies have stated that the thermal cooling to space with global warming is primarily emitted from the surface, rather than the atmosphere. Using a millennium-length coupled general circulation model (Geophysical Fluid Dynamics Laboratory's CM3) and accurate line-by-line radiative transfer calculations, here we show that the atmospheric cooling to space accounts for 12% to 50% of Earth's clear-sky longwave feedback parameter from the poles to the tropics. The atmospheric cooling to space is an efficient stabilizing feedback process because water vapor and non-condensable GHGs tend to emit at higher temperatures with surface warming as the thermodynamic structure of the atmosphere evolves. A simple yet comprehensive model is proposed in this study for predicting the clear-sky longwave feedback over a wide range of surface temperatures. It achieves good spectral agreement when compared to line-by-line calculations. Our study provides a theoretical way for assessing Earth's climate sensitivity, with important implications for Earth-like planets.

Plain Language Summary

Observations and model simulations have shown that Earth maintains a stable longwave radiative feedback process. When the surface warms by 1 K, Earth allows for 1.5 to 2.0 W/m² of extra thermal cooling to escape to space in cloud-free conditions. Recent studies have claimed that this enhanced thermal cooling to space can be explained by emissions from the surface passing through the atmosphere's infrared window. However, we find that a large portion of the stability actually results from enhanced atmospheric emission during global warming, which arises from the weakening of spectral lines broadening by radiatively inert gases (N₂, O₂, Ar) as the Earth warms. It is a well understood phenomenon in spectral physics but has been largely ignored in the feedback literature. As a result, the greenhouse effect on Earth tends to stabilize the climate, rather than initializing a runaway of thermal radiative energy. This study further proposes a simple theory for accurately predicting the clear-sky longwave feedback from climate base states.

1 Introduction

As a measure of habitability, temperature of a planet is determined by the energy balance between the absorption of sunlight and the loss of thermal heat to space. While Earth has been habitable for billions of years, its neighboring planet, Venus, has become the hottest planet in the solar system, although it may once have had liquid water and an atmosphere similar to Earth's.

Thermal cooling to space is modulated by gases that are radiatively active in the longwave (thermal) spectra via the greenhouse effect. Simpson (1928) formulated a simple model to explain thermal cooling to space when water vapor is the only greenhouse gas (GHG) as a function of surface temperature, assuming constant longwave transmission per mass of water vapor. The same assumption was used in other conceptual models (Ingersoll, 1969; Nakajima et al., 1992), which we referred to as the 'Simpsonian' model. It implies that once the longwave spectra are saturated by water vapor, surface warming results in no thermal emission to space. In this case, the planet's thermal budget would become unstable because, given enough sunlight, the ocean would evaporate continuously, causing infinite warming and a runaway greenhouse effect.

For present-day Earth, longwave spectra are nearly opaque (the atmosphere traps 88% of surface thermal emission) in the tropics, which constitutes more than one-third of the global surface area. Despite this fact, Earth is stable. In a cloud-free condition, Earth's atmosphere across the globe allows for more than 30 % of the extra thermal energy emitted from warming surfaces to escape to overcome disrupted solar or thermal energy fluxes. Thus, Earth's greenhouse effect is stable, far exceeding the prediction of a Simpsonian model.

Nevertheless, recent studies have refined the Simpsonian model and explored its implication for understanding Earth's climate (Ingram, 2010; Koll & Cronin, 2018; Jeevanjee et al., 2021), in particular, the longwave feedback, as an important measure of climate sensitivity. The longwave feedback is defined as the change in outgoing longwave radiation (OLR) per degree of surface warming. In a cloud-free condition, it is controlled by the greenhouse effect. Considering relative humidity is near-constant with surface warming (Ingram, 2010; Held & Shell, 2012; Raghuraman et al., 2019; Zhang et al., 2020), Ingram (2010) refines the Simpsonian model by treating transmission through water vapor as being constant at air temperature levels (rather than per mass throughout the column as in Simpson (1928)). With water vapor being the only GHG in this model, studies suggested that atmospheric cooling to space would be constant when the surface temperature changes. In this case, the longwave clear-sky feedback is equivalent to surface cooling to space, which is referred to as the surface Planck feedback (Koll & Cronin, 2018; Jeevanjee et al., 2021). These studies expect the clear-sky longwave feedback to be largely Simpsonian and to be qualitatively explained by the surface Planck feedback (Koll & Cronin, 2018; Jeevanjee et al., 2021).

However, much like Simpson (1928), the refined Simpsonian models do not fully explain Earth's stable climate. With observations and advanced Earth system models, the clear-sky longwave feedback is well-constrained to be -1.5 to -2.0 $\text{W}/\text{m}^2/\text{K}$ across a wide range of surface temperatures from the poles to the tropics (Koll & Cronin, 2018; Raghuraman et al., 2019; Zhang et al., 2020; Zelinka et al., 2020; Sherwood et al., 2020). In global reanalyses, the surface Planck feedback has been found to explain only -1.2 $\text{W}/\text{m}^2/\text{K}$ (63%) of the feedback (Ingram, 2013; Raghuraman et al., 2019). As surface Planck feedback vanishes to zero with increasing water vapor mass, i.e., when the runaway greenhouse effect was expected to occur (Koll & Cronin, 2018), the feedback can become even more stable, as shown in idealized simulations conducted by Seeley and Jeevanjee (2021). Therefore, a large portion of Earth's stable feedback cannot be explained by the surface cooling process in the Simpsonian models.

99 What may distinguish the stable greenhouse effect on Earth from other planets is
 100 the thermodynamic and radiative attributes of Earth’s atmosphere. They include the
 101 well-understood and observed vertical structures, the mass-conserving composition of GHGs
 102 other than water vapor, and the collision broadening between water vapor molecules and
 103 mass-conserving background gases (Goody & Yung, 1989; Clough & Iacono, 1995; Pier-
 104 rehumbert, 2010; Ingram, 2010; Paynter & Ramaswamy, 2011; Bourdin et al., 2021; See-
 105 ley & Jeevanjee, 2021; Kluft et al., 2021). Despite previous attempts in constructing partly-
 106 Simpsonian models (Ingram, 2010, 2013), it remains implicit that how these atmospheric
 107 and radiative properties interact to impact the climate sensitivity, due to the complex
 108 nature of the radiative transfer process in a changing climate. These impacts are incor-
 109 porated in a comprehensive yet simple model proposed in this study. Building upon the
 110 Simpsonian model, this conceptual model achieves quantitative accuracy in predicting
 111 the clear-sky longwave feedback parameter from the initial state of the climate. The pre-
 112 dictability of the feedback parameter relies on three key attributes of Earth’s climate sys-
 113 tem:

- 114 1. a stable thermodynamic structure of the atmosphere with a near-constant rela-
 115 tive humidity, lapse rate, and tropopause with respect to temperature.
- 116 2. an atmospheric composition dominated by radiatively inert background gas.
- 117 3. a stable atmospheric composition with conserving non-condensable GHGs and back-
 118 ground gases, as a result of physical and chemical processes within the atmosphere
 119 and its interaction with other components of the climate system

120 These attributes maintain the stable greenhouse effect on Earth.

121 2 Building upon the Simpsonian model

This section explicitly answers why Earth’s clear-sky longwave feedback is much
 more stable than a pure Simpsonian model would have expected. By definition, the clear-
 sky longwave feedback, α , is the change of OLR per degree of surface warming in cloud-
 and aerosol-free conditions. Following Goody and Yung (1989), the OLR spectra can be
 viewed as a weighted sum of thermal emissions from the surface and discretized atmo-
 spheric layers in a transmission coordinate. Similarly, we simplify the spectrally-resolved
 α as a weighted sum of thermal emission changes in the transmission coordinate (derived
 in Appendix B) (Huang & Bani Shahabadi, 2014; Feng & Huang, 2019):

$$\alpha(v) \approx \underbrace{-\pi \frac{\partial B(v, T_s)}{\partial T_s} \bar{\tau}_s(v)}_{\alpha_{\text{PL}_{\text{surf}}}(v)} \underbrace{-\pi \sum_{T'(v)}^{T_t} \mathcal{W}_i(\bar{\tau}_i(v)) [B(v, T'_i) - B(v, T_i)]}_{\alpha_{\text{Atm}}(v)} \Delta T \quad (1)$$

122 where v is the wavenumber, T_s is the surface temperature, T_t is the temperature of the
 123 tropopause. B denotes the Planck function at a given temperature. T_i , $\bar{\tau}_i$, and \mathcal{W}_i are
 124 temperature, transmission averaged over a spectral interval of δv between $v - \delta v/2$ and
 125 $v + \delta v/2$, and the weighting function of transmission for a discretized atmospheric layer
 126 at a base state before warming occurs. We use T'_i to mark the temperature of the layer
 127 where the averaged transmission reaches $\bar{\tau}_i$ when the surface temperature increases by
 128 ΔT . With $\bar{\tau}_s$ marking the vertically integrated transmission from the top-of-atmosphere
 129 (TOA) to the surface, the same transmission is reached at $T'(\bar{\tau}_s(v))$ after the warming.
 130 Feedback due to changes in transmission from an added layer between $T'(\bar{\tau}_s(v))$ and $T_s +$
 131 ΔT is negligible, as examined in Appendix B, because of the cancellation between ab-
 132 sorption and re-emission of this layer (similar to Koll and Cronin (2018)). As a result,
 133 the clear-sky longwave feedback is a sum of two terms: the change of surface Planck emis-
 134 sion transmitted by the base state atmosphere, i.e., the surface Planck feedback, denoted
 135 as $\alpha_{\text{PL}_{\text{surf}}}$; and the weighted sum of thermal emission changes at level-by-level transmis-
 136 sion within the troposphere, which is denoted as α_{Atm} and referred to as the atmospheric
 137 feedback.

138 In a Simpsonian model, where water vapor is the only GHG and the foreign pressure-
 139 broadening effect is ignored, transmission is fixed at temperature levels, thus α_{Atm} would
 140 be zero across the spectra. Therefore, Eq. 1 is consistent with existing literature that
 141 the ‘Simpsonian’ feedback is α_{PLsrf} (Koll & Cronin, 2018; Jeevanjee et al., 2021), as a
 142 result of surface cooling to space being transmitted by the vertically-integrated atmo-
 143 sphere layers, of which the vertical and temporal variations across the infrared spectra
 144 are irrelevant. Furthermore, we show that non-Simpsonian feedback caused by the ver-
 145 tical atmospheric structure and temporal variations of the transmission spectra can be
 146 analytically explained by the α_{Atm} in Eq. 1.

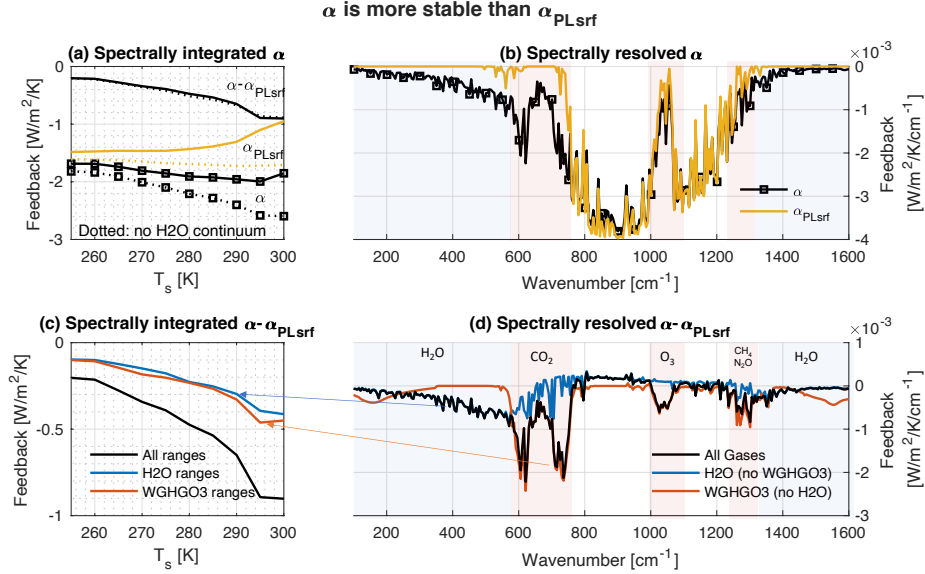


Figure 1. The clear-sky longwave feedback is more stable than that estimated by Simpsonian models, especially when the surface temperature (T_s) is high. (a) Spectrally integrated clear-sky longwave feedback α (solid black with square markers), Simpsonian feedback (surface Planck feedback α_{PLsrf} , solid yellow), and the non-Simpsonian feedback ($\alpha - \alpha_{\text{PLsrf}}$, solid black) as a function of T_s from LBL calculations. Dotted curves show feedback parameters in the absence of water vapor continuum absorption in LBL. (b) Spectrally resolved feedback parameters, α (black with square markers) and α_{PLsrf} (yellow), at 280 K surface temperature. The mean temperature-pressure profile of this region is shown in Fig. 2(a). (c) Spectrally integrated non-Simpsonian feedback over the entire infrared spectrum (black), ranges sensitive to water vapor (blue), and ranges sensitive to other GHGs (red). (d) Spectrally resolved non-Simpsonian feedback in experiments with all GHGs (black), with water vapor but no other GHGs (blue), and with well-mixed GHGs and O_3 but no water vapor (red). These experiments are described in Appendix A. Spectral ranges sensitive to water vapor and other GHGs are identified based on panel d and are marked by the blue and red shaded areas, respectively.

147 We then evaluate how well a pure Simpsonian model explains the actual clear-sky
 148 longwave feedback parameter α in a coupled global circulation model using line-by-line
 149 (LBL) calculations. Feedback parameters are shown in Fig. 1 for every 5-K bin of sur-
 150 face temperature from 252.5 to 302.5 K (covering 89 % of model grid). The surface Planck
 151 feedback, α_{PLsrf} , is determined by two factors: the derivative of Planck function ($\frac{\partial B(v, T_s)}{\partial T_s}$)
 152 and the vertically integrated transmission of the GHGs ($\bar{\tau}_s(v)$, inferred from LBL) at

153 the base state. While the former increases with T_s due to Planck's law, transmission through
 154 water vapor decays with T_s . With only line absorption (dotted curves in Fig. 1(a)), $\alpha_{\text{PL}_{\text{srf}}}$
 155 is almost constant with T_s , indicating that the T_s^4 growth of the Planck function is can-
 156 celled out by line absorption with increasing water vapor path. As continuum absorp-
 157 tion increases with specific humidity, transmission decays more dramatically when both
 158 line and continuum absorption are included (solid curves in Fig. 1(a)), so that the ac-
 159 tual $\alpha_{\text{PL}_{\text{srf}}}$ increases (less negative) with T_s . In contrast, the clear-sky longwave feedback,
 160 α , tends to decrease with T_s rather than increase with it. Regardless of water vapor con-
 161 tinuum, the discrepancy between α and $\alpha_{\text{PL}_{\text{srf}}}$, as the non-Simpsonian feedback, takes
 162 about -0.2 (12% of α at 255 K T_s) to -0.9 $\text{W}/\text{m}^2/\text{K}$ (50% of α at 300 K T_s) of the feed-
 163 back parameter. Similar statistics have been noted in Raghuraman et al. (2019) based
 164 on reanalysis of present-day Earth. Thus it would appear that a pure Simpsonian model
 165 (Ingram, 2010; Koll & Cronin, 2018; Jeevanjee et al., 2021) can not explain the magni-
 166 tude of the feedback parameter, nor its dependence upon T_s . In particular, it seems to
 167 underestimate the stability of α at high T_s .

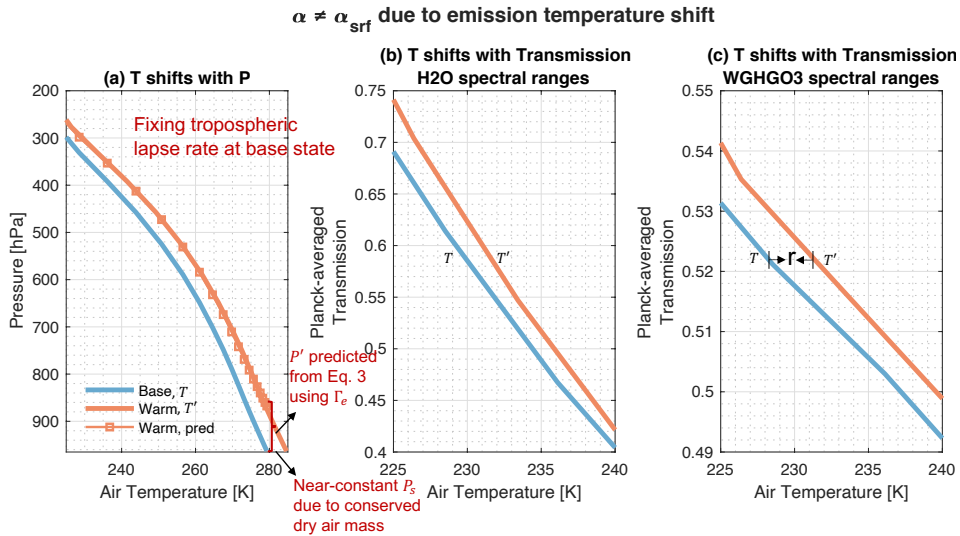


Figure 2. (a) Temperature-pressure profile in the base state (blue) and warm state (red). Red squares mark the shifted temperature-pressure profile predicted based on Eq. 3 using pseudo-adiabatic lapse rate Γ_e . (b): averaged transmission over spectral ranges sensitive to water vapor line absorption, from TOA to a given tropospheric air temperature (blue-shaded area in Fig. 1(b,c)) in the base state at 280 K surface temperature (blue) and the warmed state at 285 K surface temperature (red), holding RH fixed. (c) the same as (b) but over spectral ranges sensitive to well-mixed GHGs and O_3 (red-shaded area in Fig. 1(b,c)).

168 Furthermore, the spectrally-decomposed feedback parameter at 280 K T_s suggests
 169 that a pure Simpsonian model cannot fully explain α across infrared channels (Fig. 1(a)),
 170 in line with the feedback spectra from idealized simulations at surface temperatures warmer
 171 than 305 K (Seeley & Jeevanjee, 2021; Kluff et al., 2021). First, we note that the non-
 172 Simpsonian feedback is positive in the water vapor window (800 to 1000 cm^{-1}), as a re-
 173 sult of the difference between the trapped surface thermal emission by the new atmo-
 174 sphere layer between $T'(\bar{\mathcal{T}}_s(v))$ and $T_s + \Delta T$ and the emission of this layer. It integrates
 175 to within 0.05 $\text{W}/\text{m}^2/\text{K}$, confirming that the non-Simpsonian feedback is dominated by
 176 α_{Atm} in Eq. 1. We further investigate how the break-down of temperature-transmission
 177 relation leads to the substantial, negative α_{Atm} in absorption channels. Transmission at

178 temperature levels depends on the mass of absorbers and the absorption coefficient per
 179 mass. On the one hand, the radiative effect of GHGs other than water vapor, including
 180 CO₂, CH₄, N₂O, O₃, are not considered in a pure Simpsonian model. The mass of these
 181 GHGs in the troposphere tends to be proportional to the total air mass rather than fixed
 182 at temperature levels. Consequently, these GHGs become more transparent to infrared
 183 radiation (Fig. 2(c)), contributing to the negative feedback ($T'_i > T_i$ in Eq. 1). Such
 184 impact has been expected by existing literature (Ingram, 2010; Jeevanjee et al., 2021)
 185 as the main source of non-Simpsonian feedback, although here we find only half of the
 186 non-Simpsonian feedback is explained by spectral ranges sensitive to these GHGs (the
 187 red-shaded area in Fig. 1). On the other hand, at the same air temperature, absorption
 188 coefficient per mass in spectral ranges away from a saturated line center decreases when
 189 molecules of water vapor and other GHGs collide less often with N₂ and O₂ with sur-
 190 face warming. Consequently, water vapor (of the same mass) becomes more transpar-
 191 ent to infrared radiation (Fig. 2(b)), causing negative feedback. Figure 1(c) shows that
 192 feedback in water vapor absorption channels, as a result of the collision-broadening ef-
 193 fect (Ingram, 2010, 2013), accounts for the other half of the non-Simpsonian feedback
 194 between 255 and 300 K T_s .

195 3 Emission temperature shift theory

196 Section 2 shows that a pure Simpsonian model cannot explain the magnitude of
 197 clear-sky longwave feedback, α , nor its dependence upon surface temperature, because
 198 it ignores the non-constant relationship between temperature and transmission. Atmo-
 199 spheric feedback, α_{Atm} , is proposed to explain the non-Simpsonian feedback as a result
 200 of the shifting temperature in the transmission coordinate with surface warming (Eq.
 201 1).

An 'emission temperature shift ratio' is defined to quantify the shifting tempera-
 ture in transmission coordinate in Eq. 1 :

$$r = \frac{T'_i}{T_i}$$

Considering temperature shifts uniformly with respect to transmission in Fig. 2, we may
 assume r at a given wavenumber to be vertically uniform and then substitute $T'_i = rT_i$
 into Eq. 1:

$$\begin{aligned} \alpha_{\text{Atm}}(v) &= -\pi \frac{\sum_{T'}^{T_t} \mathcal{W}_i(\bar{\mathfrak{x}}_i(v)) [B(v, rT_i) - B(v, T_i)]}{\Delta T} \\ &\approx -R_{\text{trop}}(v) \frac{B(v, rT_e(v)) - B(v, T_e(v))}{R(v)} \end{aligned} \quad (2)$$

where $B(v, T_e(v)) \equiv R(v)$

202 where $R(v)$ is the OLR at wavenumber v , and $R_{\text{trop}}(v)$ is the OLR sourced from tro-
 203 posphere at v , respectively (see Eq. B1 for the decomposition of OLR). In this expres-
 204 sion, we consider that $\alpha_{\text{Atm}}(v)$ can be adequately represented by the change of black-
 205 body emission temperature from $T_e(v)$ to $rT_e(v)$ with an emissivity of $\frac{R_{\text{trop}}(v)}{R(v)}$. Hence,
 206 the magnitude of α_{Atm} is controlled by $R_{\text{trop}}(v)$, as given by radiative transfer at the
 207 base state, and r .

208 The emission temperature shift ratio, r , is jointly determined by layer-by-layer air
 209 temperature, partial pressure of background gases (foreign pressure), and partial pres-
 210 sure of every GHG in the base state atmosphere, as well as their impacts on the layer-
 211 by-layer transmittance spectra with surface warming. Despite the complexity, r can be
 212 inferred from the base state if the change of these properties with surface warming fol-
 213 lows a predictable pattern. And it does, as a consequence of basic thermodynamic re-
 214 lations.

215 First, temperature and pressure are linked via the temperature lapse rate, Γ , under
 216 the hydrostatic balance, based on the barometric formula:

$$P_i = P_s \left[\frac{T_i}{T_s} \right]^A, \quad A = \frac{g}{R\Gamma},$$

217 where g is gravity and R is the specific gas content of the air. P_s is surface pressure and
 218 is considered to be constant with warming because the dry air mass, which consists of
 219 more than 98% of the atmosphere, is conserved.

When the surface warms from T_s to T'_s , if the mean lapse rate from T_s to the tropopause
 changes little in this process (see Fig. 2 (a)) (Ingram, 2010), we may infer the air pressure
 at T_i changes from P_i to P'_i :

$$\begin{aligned} P'_i &= P_s \left[\frac{T_s}{T'_s} \right]^{A(\Gamma_e)} \left[\frac{T_i}{T_s} \right]^{A(\Gamma')} \\ &= P_i \left[\frac{T_s}{T'_s} \right]^{A(\Gamma_e)}, \quad \text{when } \Gamma' = \Gamma \end{aligned} \quad (3)$$

220 An 'effective' lapse rate, Γ_e , is used to describe the change of air pressure at a given T_i
 221 with warming. Assuming the bottom of atmosphere expands pseudo-adiabatically under
 222 fixed RH with the surface warming, Γ_e is then the pseudo-adiabatic lapse rate from
 223 T_s to T'_s . Although it is a crude assumption without considering heat transfer or dynam-
 224 ical transport, it captures the shifting temperature-pressure relationship with warming,
 225 as illustrated in Fig. 2(a).

Furthermore, partial pressure of water vapor and other GHGs are physically linked
 to air temperature and air pressure, respectively. While the partial pressure of well-mixed
 GHGs, by definition, is fixed at pressure levels, we may treat tropospheric O_3 similarly.
 The partial pressure of water vapor, P_{gas_q} , is a function of air temperature via the Clausius-
 Clapeyron (CC) equation, given that RH is near-constant (Zhang et al., 2020). We fur-
 ther simplify the CC equation using a linear coefficient k_{CC} to represent P_{gas_q} at relative-
 humidity \mathcal{RH} :

$$P_{gas_q,i} = \mathcal{RH} e^{k_{CC} T_i}$$

Therefore, the change of air temperature, foreign pressure, and partial pressure of
 every GHG with surface warming can be inferred from their base states. For line absorp-
 tions of an individual GHG, the impacts of these quantities on transmittance caused by
 a saturated line over a spectral interval (i.e., 1 cm^{-1}) can be simplified using a regres-
 sion coefficient by adopting a strong-line approximation (Goody & Yung, 1989; Pierre-
 humbert, 2010), as described in Eq. C2. Assuming a random overlap of lines of each GHG,
 r can be approximately solved as (Appendix C):

$$\begin{aligned} r(v) &\approx \frac{\mathcal{F}_1 + \mathcal{F}_2}{\frac{\mathcal{F}_1}{T'_s} + \mathcal{F}_2} + \frac{2 \sum_G f_G + f_{ql}}{T_e (\frac{\mathcal{F}_1}{T'_s} + \mathcal{F}_2)} \ln \frac{T'_s}{T_s} [A(\Gamma_e) - A(\Gamma)], \\ &\text{where } G = \text{CO}_2, \text{CH}_4, \text{N}_2\text{O}, \text{ and } \text{O}_3 \\ \mathcal{F}_1 &= (2 \sum_G f_G + f_{ql}) A(\Gamma) - (\sum_G f_G + f_{ql} + f_{qc}), \\ \mathcal{F}_2 &= (2f_{qc} + f_{ql}) k_{CC} + f_{\text{CO}_2} k_l \end{aligned} \quad (4)$$

226 where the subscript 'ql' refers to water vapor line absorptions, 'qc' refers to water vapor
 227 vapor continuum absorptions, 'G' refers to line absorptions of other GHGs. f_G , f_{ql} and f_{qc}
 228 are inferred from the regression coefficients for each mechanism at every wavenumber
 229 (Eq. C10 in Appendix C). These coefficients are obtained from LBL calculations per-
 230 formed at a reference state and are included in the Supplementary. k_l is a line intensity
 231 parameter for CO_2 , which is set to 0.02 in this study. A simpler form of this equation
 232 can be found in Eq. C3 and C6 for an individual GHG. With $k_{CC} \approx 0.09$ and $A(\Gamma) \approx$

233
234
235

5.26 at 280 K, the magnitude of r is mainly controlled by the ratio of surface warming $\frac{T'_s}{T_s}$, the effect of foreign pressure $2\sum_G f_G + f_{ql}$ versus air temperature $2f_{qc} + f_{ql}$, and Γ_e .

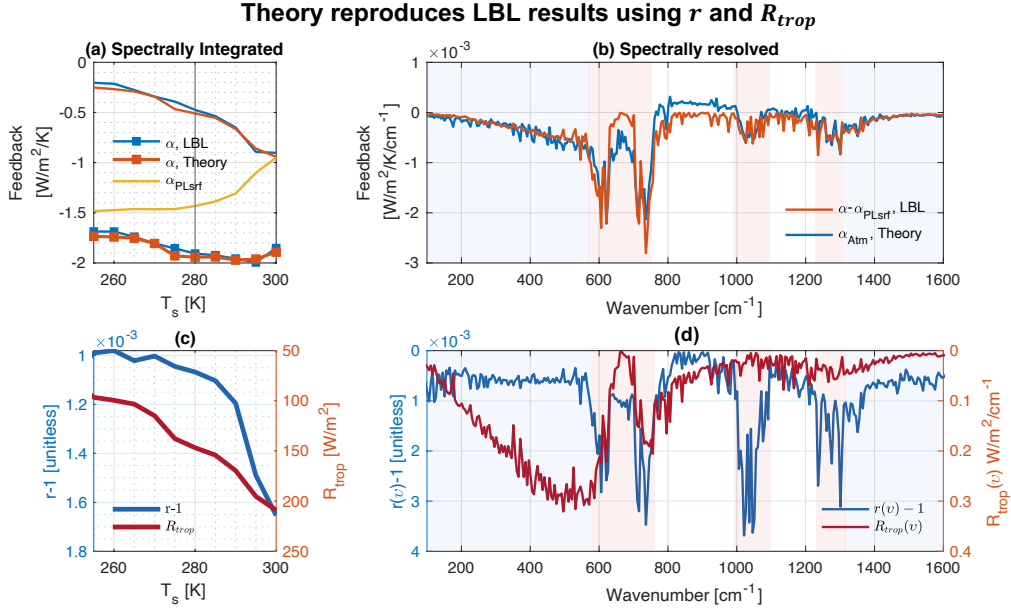


Figure 3. Feedback parameters predicted from Eq. 2 and 4 match well with line-by-line calculations, using the emission temperature shift ratio, r , and the OLR sourced from troposphere, R_{trop} . (a): clear-sky longwave feedback (α , solid curve with square markers), non-Simpsonian feedback from line-by-line calculations (blue) and from theoretical predictions (red), and surface Planck feedback (yellow). (b): similar to left panels but for spectrally decomposed non-Simpsonian feedback ($\alpha(v) - \alpha_{PLsrf}(v)$ from LBL and $\alpha_{Atm}(v)$ from theory) at 280 K T_s , convoluted from 1 cm⁻¹ to 5 cm⁻¹. (c) $r - 1$ for 1 K of surface warming estimated from Eq. 2 in the left axis (blue) and the OLR sourced from troposphere (R_{trop}) in the right axis (right). (d) is the same as (c) but for spectrally-resolved $r - 1$ and R_{trop} .

236
237
238
239
240
241
242
243
244
245
246
247
248
249

Equations 2 and 4 are combined to estimate the the atmospheric feedback, α_{Atm} , which are further summed with the surface Planck feedback, α_{PLsrf} , for the total feedback, α . Only temperature and partial pressure of gases at the base state are used, in addition to the LBL-derived regression coefficients at a reference state. The results match well with LBL for a wide range of surface temperature from 255 to 300 K, as presented in Fig. 3(a). Figure 3(b) further shows the spectrally-resolved α_{Atm} at 280 K surface temperature as an example. There is negative bias in [800 1000] cm⁻¹ caused by the neglected surface transmission change ($\alpha_{\Delta\tau_s}$ in Eq. B3) and positive bias around 650 cm⁻¹ in the center of CO₂ absorption channel caused by the neglected stratospheric feedback ($\frac{\partial R_{strat}}{\partial T_s}$ in Eq. B2 and see Fig. C2 for validation of tropospheric feedback). Biases in the two spectral ranges are small and cancel out after spectral integration. In essence, the good agreement with line-by-line calculations confirms that the model proposed in Eq. 1, 2 and 4 covers key process and/or relations that affects the clear-sky longwave feedback. In the following context, the simple model is used to understand the feedback comprehensively.

250
251
252

For well-mixed GHGs and O₃ (the red-shaded area in Fig. 3(b,d)), α_{Atm} is caused by the increases of Planck function at constant mass of these gases. In the absence of water vapor, this feedback process is straightforward to be understood and has been viewed

253 as the 'Planckian-like' feedback by Ingram (2010), with r being approximately $\frac{T'_s}{T_s}$ (0.0036
 254 in Fig. 3(d)). Here we further relate the Planck function to transmission and show that
 255 the spectral pattern of α_{Atm} is controlled by r when overlaps with the broad water vapor
 256 absorption spectrum in regions with different atmospheric conditions (Fig. 3(a,b)).
 257 Moreover, α_{Atm} in O_3 absorption spectrum is well predicted when O_3 is treated as well-
 258 mixed tropospheric gases in Eq. 4. While O_3 increases the opacity of the water vapor
 259 window around 1080 cm^{-1} to result in less negative α_{PLstrf} , our results suggest that the
 260 atmospheric feedback due to thermal emissions of stratospheric O_3 is negligible and that
 261 the role of O_3 is similar to well-mixed GHGs in stabilizing the clear-sky longwave feed-
 262 back.

263 For water vapor (the blue-shaded area in Fig. 3), α_{Atm} is substantial and is spec-
 264 trally integrated into half of the non-Simpsonian feedback. This result is counter-intuitive,
 265 as Simpsonian models expected zero emission temperature shift from the exponential CC
 266 relation, which was considered to outweigh the foreign pressure-broadening effect. Here
 267 we show that in water vapor absorption channels, the magnitude of $r-1$ is reduced to
 268 not zero, but roughly 20% of $\frac{T'_s}{T_s}$. Although r is smaller compared to other GHGs (blue
 269 curve in Fig. 3(d)), greater thermal energy is emitted from water vapor channels (R_{trop} ,
 270 red curve in Fig. 3(d)) because 1) water vapor absorption is strong in the troposphere
 271 to mask over surface emissions but weaker in the stratosphere to transmit tropospheric
 272 emissions, and 2) Planck function at tropospheric temperature peaks within the water
 273 vapor rotational-vibrational spectrum. Thus water vapor can contribute half of α_{Atm} ow-
 274 ing to the compensation from greater tropospheric emission.

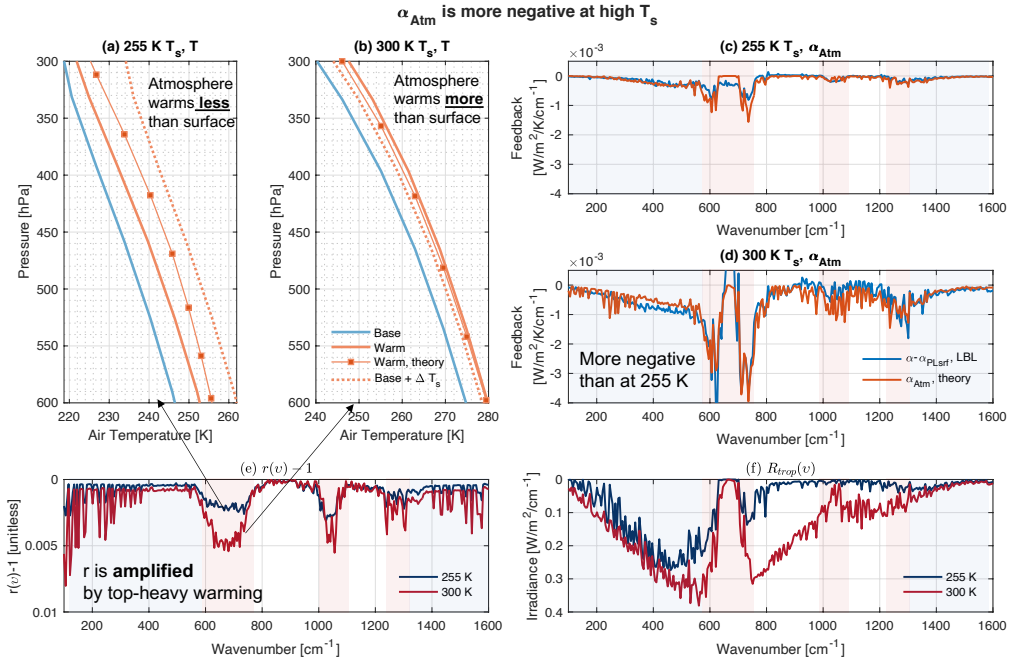


Figure 4. α_{Atm} is amplified by the emission temperature shift ratio, r , at high surface temperature due to the pseudo-adiabatic thermal expansion. Panels (a) and (c) are similar to Fig. 2(a) and Fig. 3(b), respectively, at 255 K surface temperature. Panels (b) and (d) are the same as (a) and (c) but at 300 K surface temperature. (e) Spectrally resolved $r-1$ per 1 K of surface warming at 255 K (blue) and 300 K (red) surface temperature. (f) Spectrally resolved R_{trop} at 255 K (blue) and 300 K (red) surface temperature.

275 Importantly, we find that the clear-sky longwave feedback, α , maintains a range
 276 between -1.5 to -2.0 $W/m^2/K$ because α_{Atm} becomes more negative at high T_s to com-
 277 pensate for vanishing $\alpha_{\text{PL}_{\text{srf}}}$, rather than being explained by $\alpha_{\text{PL}_{\text{srf}}}$ alone (Koll & Cronin,
 278 2018). This dependence of α_{Atm} upon surface temperature is robust regardless of the com-
 279 bination of GHGs in radiative calculations (Fig. C2). We elucidate in Fig. 4 that α_{Atm}
 280 enhances across all absorption channels with surface temperature because two factors.
 281 First, more tropospheric emission is radiated to TOA at a higher surface temperature
 282 in weak absorption channels, where OLR is more sensitive to emissions from the lower
 283 troposphere (R_{trop} , Fig. 4(d)). It partly explains α_{Atm} in radiative fins of GHGs. Sec-
 284 ond, the emission temperature shift increases substantially with surface temperature (r ,
 285 Fig. 4(e)). It is responsible for more negative α_{Atm} at 300 K than at 255 K across all
 286 absorption channels. This is because r accounts for different tropospheric warming struc-
 287 tures from the poles to the tropics. If the troposphere warms more than the surface, as
 288 in the tropical region (at 300 K in Fig. 4), there would be a greater temperature shift
 289 in pressure coordinate and hence in transmission coordinate, thus amplifying r and α_{Atm} .
 290 Such effect is characterized by the pseudo-adiabatic thermal expansion using Γ_e in this
 291 study. This crude approximation generally captures the warming structure in the up-
 292 per and middle troposphere (Fig. 4(a,b)) and facilitates an accurate feedback prediction
 293 across different base states (surface temperatures) without knowing actual temperature
 294 profiles in the warm states.

295 We note that although the impact of RH is implicit in Eq. 1 or Eq. 4, the column-
 296 mean RH, as well as the vertical RH structure, are important for the state-dependent
 297 clear-sky longwave feedback parameters. While the column-mean RH affects the $\alpha_{\text{PL}_{\text{srf}}}$
 298 via the vertically-integrated transmittance of the base state atmosphere ($\bar{\tau}_s$) (Koll & Cronin,
 299 2018; McKim et al., 2021), the vertical RH structure affects the α_{Atm} (Bourdin et al.,
 300 2021) via the contribution from water vapor (f_{ql} and f_{qc} , which depend on vapor pres-
 301 sure in Eq. C10) and the OLR across infrared spectra. A spectrally varying effective RH,
 302 determined from the vertical levels where T_e is located, is used to produce Fig. 3 and
 303 4. Therefore, RH controls these base-state quantities ($\bar{\tau}_s$, P_q , R_{trop} , and T_e) and should
 304 be treated carefully.

305 4 Discussion

306 Based on line-by-line radiative transfer calculations and a millennium-length cou-
 307 pled general circulation model, this study presents a novel, simple theory to explain the
 308 effect of greenhouse gases (GHGs) on outgoing longwave radiation (OLR) for quantita-
 309 tively evaluating clear-sky longwave feedback. This theory proposes that the complex
 310 clear-sky longwave feedback can be viewed as a sum of two processes (Eq. 1): 1) feed-
 311 back due to surface cooling to space, $\alpha_{\text{PL}_{\text{srf}}}$, which only depends on surface temperature
 312 and the total transmission through the atmosphere; and 2) feedback due to atmospheric
 313 cooling to space, α_{Atm} , which depends on the thermodynamic structure and gas com-
 314 position within the atmosphere. We further show that the frequently ignored α_{Atm} sources
 315 from increased emission temperatures with warming caused by the well-understood collision-
 316 broadening effect and the presence of well-mixed GHGs and O_3 . The α_{Atm} decreases from
 317 -0.2 $W/m^2/K$ at 255 K to -0.9 $W/m^2/K$ at 300 K, the magnitude of which is quanti-
 318 tatively predicted by the emission temperature shift theory via pseudo-adiabatic lapse
 319 rates (Eq. 4). In the absence of α_{Atm} , the clear-sky longwave feedback would increase
 320 from -1.5 $W/m^2/K$ at 255 K to -0.9 $W/m^2/K$ at 300 K because water vapor continuum
 321 absorption increases the $\alpha_{\text{PL}_{\text{srf}}}$ (Fig. 1). Thus, without α_{Atm} , the clear-sky longwave feed-
 322 back parameter would be only half as stable as it is, which is the source of the paradox
 323 found in Simpson (1928). We conclude that GHGs induce an atmospheric feedback pro-
 324 cess that critically stabilizes Earth's climate.

325 As a sum of the two processes, clear-sky longwave feedback of Earth can be accu-
 326 rately predicted from base states of surface temperatures and atmospheric conditions us-

327 ing the simple, analytical model proposed in this study (Eq. 1 and 2). In a climate hot-
 328 ter than Earth’s tropics (i.e., 300 K in Fig. 4(b,d)), our study suggests that α_{Atm} alone
 329 explains the clear-sky longwave feedback since $\alpha_{\text{PL}_{\text{srf}}}$ would vanish to zero (Koll & Cronin,
 330 2018; Seeley & Jeevanjee, 2021). With the magnitude of α_{Atm} controlled by tropospheric
 331 cooling to space (R_{trop}) and emission temperature shift (r), α_{Atm} would become more
 332 negative (stable) than the $-0.9 \text{ W/m}^2/\text{K}$ because 1) R_{trop} increases with tropospheric
 333 temperature and 2) r is enhanced by a steeper pseudo-adiabatic lapse rate (Γ_e), which
 334 gives rise to stronger upper-tropospheric warming than the surface. The sensitivity to
 335 the upper troposphere can be further amplified if CO_2 mass increases with surface warm-
 336 ing, as shown in Seeley and Jeevanjee (2021). While Kluft et al. (2021) has questioned
 337 the effectiveness of CO_2 on the feedback process, it is evident in our study that the pres-
 338 ence of CO_2 is not required for the negative atmospheric feedback process at all, because
 339 the negative feedback process is sufficiently maintained by water vapor via the collision-
 340 broadening with nitrogen and oxygen in the absence of any other GHGs (Fig. 1(d), and
 341 Fig. C2(e,f) compared to Fig. C2(c,d)).

342 Importantly, the stability and predictability of the clear-sky longwave feedback rely
 343 on the robust, near-constant relative humidity, lapse rate, and tropopause at tempera-
 344 ture levels with surface warming (Ingram, 2010; Held & Shell, 2012). In this process, the
 345 mass of non-condensable gases is well-maintained by the atmosphere and other compo-
 346 nents of the climate system. As long as a similar evolving thermodynamic pattern is ex-
 347 hibited, the theory presented in this study is generalizable to past, present, and future
 348 climates of Earth, as well as other planets. At the time of longwave saturation, any break-
 349 down of this pattern might trigger a runaway greenhouse effect, either locally, season-
 350 ally, or globally. Thus, our study suggests that the runaway greenhouse effect occurs con-
 351 ditionally, rather than unconditionally (Nakajima et al., 1992; Ingersoll, 1969). While
 352 Earth-like climate may become unstable given sufficiently high radiation disruptions (e.g.,
 353 from insolation or anthropogenic emissions) in simulations with idealized thermodynamic
 354 pattern (Goldblatt et al., 2013), our results indicate that such runaway might initiate
 355 from a surface temperature much higher than present-day Earth (i.e., at and beyond the
 356 boiling point) so that the foreign pressure-broadening effect becomes weak enough (high
 357 saturation vapor pressure versus conserved background gases) to be overcome by posi-
 358 tive shortwave feedback from clouds, albedo, and water vapor. These conditions should
 359 be examined with care in future studies when addressing the emergence of the runaway
 360 greenhouse effect on Earth and other Earth-like planets.

361 Appendix A Data and Experiment

362 Two experiments are conducted with the Geophysical Fluid Dynamics Laboratory
 363 (GFDL)’s CM3 (Donner et al., 2011; Griffies et al., 2011) in Paynter et al. (2018). The
 364 first is a control run, where CO_2 is fixed at a pre-industrial level, and the second is an
 365 experiment run, where CO_2 increases by 1% per year until reaching a doubling, and then
 366 CO_2 is held constant until equilibrium with the control run is reached. We evaluate these
 367 two runs at the equilibrium state (approximately 4.8 K of warming, 4800 years after CO_2
 368 doubling).

369 Every grid point from the control run is composited into every 5-K bin of surface
 370 temperature. Figures in this study show bins from 252.5 to 302.5 K, covering 89% of these
 371 grids. Mean profiles of each bin are obtained from both the control and the experimen-
 372 tal run. Using these composited profiles, a set of radiative transfer calculations is con-
 373 ducted. Spectrally-resolved gas optical depths are calculated using a new benchmark line-
 374 by-line model, pyLBL (<https://github.com/GRIPS-code/pyLBL>). This python-based model
 375 downloads up-to-date line-by-line data from the HITRAN database and uses MT-CKD
 376 3.5 continuum coefficients. Using the optical depths, longwave fluxes are calculated with
 377 a diffusivity factor of 1.66.

378 Four experiments are conducted to decompose the longwave radiative feedback:

- 379 • a) atmospheric profiles and surface temperature from the control run.
- 380 • b) atmospheric profiles and surface temperature from the experimental run.
- 381 • c) temperature profiles and surface temperature from the experimental state while
- 382 holding relative humidity fixed at the control run.
- 383 • d) temperature profiles and surface temperature from the experimental state while
- 384 holding profiles above the cold-point tropopause of the control run fixed.

385 Experiment a is used as the 'base state' and experiment b is used as the 'warm state'
 386 in this study. The clear-sky longwave feedback is estimated from the difference in OLR
 387 between the a and b, as shown in Fig. 3. We find that the feedback estimated from c-
 388 a is similar to b-a, confirming that RH feedback is small from a global-mean perspec-
 389 tive (Held & Shell, 2012). Experiment d is used in Appendix C for validating Eq. 1, in
 390 which feedback sourced from the stratosphere is manually neglected.

391 These LBL calculations are driven by three combinations of greenhouse gases and
 392 an experiment that excludes water vapor continuum absorption:

- 393 1. 'All gases': water vapor and O₃ profiles and well-mixed CO₂, N₂O, CH₄ at the
 394 pre-industrial gas level.
- 395 2. 'WGHGO3': O₃ profile and well-mixed CO₂, N₂O, and CH₄ (without water va-
 396 por).
- 397 3. 'H2O': water vapor line and continuum absorption (without other GHGs).
- 398 4. 'noctm': water vapor line absorptions, O₃ profile and well-mixed CO₂, N₂O, CH₄
 399 at the pre-industrial gas level.

400 Background gases, including N₂ and O₂, are hold constant at fixed numbers of molecules,
 401 regardless of the combinations of greenhouse gases.

402 Appendix B Derivation of feedback decomposition

403 At a surface temperature, T_s , spectrally-resolved longwave flux at TOA ($R(\nu)$) can
 404 be decomposed as a weighted sum of contributions from surface and discretized atmo-
 405 spheric layers (Goody & Yung, 1989):

$$\begin{aligned}
 OLR &= \int_{\nu} R(\nu) d\nu \\
 R(\nu) &= R_{\text{srf}}(\nu) + R_{\text{trop}}(\nu) + R_{\text{strat}}(\nu) \\
 &\approx \pi B(\nu, T_s) \bar{\mathfrak{T}}_s(\nu) + \pi \sum_{T_b}^{T_t} B(\nu, T_i) \mathcal{W}_i(\bar{\mathfrak{T}}_i(\nu)) + R_{\text{strat}}(\nu)
 \end{aligned} \tag{B1}$$

406 where T_i is the atmospheric temperature of a discrete layer and B is the Planck func-
 407 tion of a given temperature. At ν , the averaged-transmission and weighting function of
 408 this discrete layer are denoted as $\bar{\mathfrak{T}}_i$ and \mathcal{W}_i , respectively. $\bar{\mathfrak{T}}_s(\nu)$ describes the averaged
 409 transmission between $\nu - \delta\nu/2$ and $\nu + \delta\nu/2$ from surface to space, with $\delta\nu$ being 1 cm^{-1} .
 410 If the temperature monotonically decreases from the bottom of the atmosphere to the
 411 tropopause, T_i , \mathcal{W}_i , and $\bar{\mathfrak{T}}_i$ are unambiguously mapped to one another at every frequency
 412 (Huang & Bani Shahabadi, 2014; Feng & Huang, 2019). T_t and T_b then mark the tem-
 413 perature of the bottom and the top of the troposphere. R_{trop} and R_{strat} are used to rep-
 414 resent the sum of tropospheric and stratospheric contribution to $R(\nu)$, respectively.

The clear-sky longwave feedback α is defined as the change in clear-sky OLR per degree of surface warming. At a frequency ν , we express $\alpha(\nu)$ as:

$$\begin{aligned}
 \alpha(\nu) &= -\frac{\partial R(\nu)}{\partial T_s} = -\frac{\partial R_{\text{srf}}(\nu)}{\partial T_s} - \frac{\partial R_{\text{trop}}(\nu)}{\partial T_s} - \frac{\partial R_{\text{strat}}(\nu)}{\partial T_s} \\
 -\frac{\partial R_{\text{srf}}(\nu)}{\partial T_s} &\approx -\pi \frac{B(\nu, T'_s)[1 - \mathcal{A}(\nu)]\bar{\tau}'_s(\nu) - B(\nu, T_s)\bar{\tau}_s(\nu)}{\Delta T_s} \\
 -\frac{\partial R_{\text{trop}}(\nu)}{\partial T_s} &\approx -\pi \frac{\sum_{T'_b}^{T_t} B(\nu, T'_i)\mathcal{W}_i(\bar{\tau}_i, \nu) - \sum_{T_b}^{T_t} B(\nu, T_i)\mathcal{W}_i(\bar{\tau}_i, \nu)}{\Delta T_s} \\
 &\quad - \pi \frac{\sum_{T'_s}^{T'(\bar{\tau}_s(\nu))} B(\nu, T'_i)\mathcal{A}(\nu)\bar{\tau}'_s(\nu)}{\Delta T_s} \\
 -\frac{\partial R_{\text{strat}}(\nu)}{\partial T_s} &\approx 0
 \end{aligned} \tag{B2}$$

where the superscript $'$ denotes the state after the warming. The warmed atmosphere reaches $\bar{\tau}_s(\nu)$ at $T'(\bar{\tau}_s(\nu))$. The emissivity from this layer to the warmed surface is denoted as \mathcal{A} . $\mathcal{A}\bar{\tau}'_s$ then is equivalent to the weighting \mathcal{W} of the of layer from $T'(\bar{\tau}_s(\nu))$ to T'_s . If $\bar{\tau}_s$ increases in a warmer climate, this expression mathematically creates a pseudo layer from T'_s to $T'(\bar{\tau}_s(\nu))$. Adjustments of the stratosphere with surface warming are not considered in the feedback process we discuss here. We can then regroup Eq. B2 into three terms: surface (PL_{srf}), atmosphere (Atm), and the change of atmospheric transmittance ($\Delta\bar{\tau}_s$):

$$\alpha(\nu) = \alpha_{\text{PL}_{\text{srf}}}(\nu) + \alpha_{\text{Atm}}(\nu) + \alpha_{\Delta\bar{\tau}_s}(\nu)$$

where:

$$\begin{aligned}
 \alpha_{\text{PL}_{\text{srf}}}(\nu) &= -\pi \frac{\partial B(\nu, T_s)}{\partial T_s} \bar{\tau}_s(\nu) \\
 \alpha_{\text{Atm}}(\nu) &= -\pi \frac{\sum_{T'_b}^{T_t} \mathcal{W}_i(\bar{\tau}_i, \nu)[B(\nu, T'_i) - B(\nu, T_i)]}{\Delta T} \\
 \alpha_{\Delta\bar{\tau}_s}(\nu) &= -\pi \frac{\sum_{T'_s}^{T'(\bar{\tau}_s(\nu))} [B(\nu, T'_i) - B(\nu, T_s)]\mathcal{A}(\nu)\bar{\tau}'_s(\nu)}{\Delta T_s} \approx 0
 \end{aligned} \tag{B3}$$

415 In this expression, the magnitude of $\alpha_{\Delta\bar{\tau}_s}(\nu)$ is small compared to $\alpha_{\text{PL}_{\text{srf}}}(\nu)$ in either
 416 optically thick or thin channel, because the absorption of surface thermal emission of the
 417 layer between T'_s and $T'(\bar{\tau}_s(\nu))$ is close to the thermal emission of this layer ($|B(\nu, T'(\bar{\tau}_s(\nu))) -$
 418 $B(\nu, T'_s)| < B(\nu, T_s + \Delta T) - B(\nu, T_s)$ and $\mathcal{A}(\nu)\bar{\tau}'_s(\nu) < \bar{\tau}_s(\nu)$). Hence, the feedback
 419 $\alpha(\nu)$ is approximately the sum of surface term $\alpha_{\text{PL}_{\text{srf}}}(\nu)$ and atmospheric term $\alpha_{\text{Atm}}(\nu)$,
 420 giving Eq. 1.

421 Appendix C Derivation of atmospheric emission temperature shift

Following Eq. 4.15 in Goody and Yung (1989) (Goody & Yung, 1989) and Eq. 4.69 in Pierrehumbert (2010) (Pierrehumbert, 2010), the averaged transmission between $\nu - \delta\nu/2$ and $\nu + \delta\nu/2$ due to a strong gas line is proportional to the square root of the prod of $\frac{P_i}{T_i}$, collision-broadened line width, and line intensity:

$$\bar{\tau}_{G,i}(\nu) \approx 1 - \bar{k}_G(\Gamma, \nu) \left[\frac{P_i P_{\text{gas},i}}{T_i} e^{k_i T_i} \right]^n, n = \frac{1}{2} \tag{C1}$$

422 where $\bar{\tau}_{G,i}(\nu)$ is the averaged transmission between $\nu - \delta\nu/2$ and $\nu + \delta\nu/2$. P_i and T_i
 423 are the air pressure and temperature at a discrete layer. $P_{\text{gas},i}$ is the partial pressure
 424 of the gas specie G . This approximation is obtained by integrating over the far-tail of
 425 Lorentz profile (Goody & Yung, 1989; Pierrehumbert, 2010). Here we assume that the
 426 width of the Lorentz profile collision broadening is proportional to P_i and independent

427 of T_i and the line intensity is proportional to $e^{k_l T_i}$. This k_l is taken to be 0.02 for CO_2
 428 but zero otherwise due to 1) a low concentration of other well-mixed gases on Earth, and
 429 2) a much stronger impact from the temperature dependence of saturation vapor pres-
 430 sure. The validity of Eq. C1 is examined in Fig. C1 using water vapor absorption as an
 431 example. It shows that $\bar{\mathfrak{T}}_{G,i}(v)$ is near-equally contributed by partial pressure and for-
 432 eign pressure and that $\bar{\mathfrak{T}}_{G,i}(v)$ is roughly proportional to $\frac{P_i P_{gas,G,i}}{T_i}$ when k_l is taken to
 433 be zero.

In the following derivation, we treat $\bar{k}_G(\Gamma, v)$ as a parameter by assuming a con-
 stant lapse rate over a certain vertical range. At each wavenumber, this \bar{k}_G can be then
 empirically estimated as:

$$\bar{k}_G(v) = \frac{\partial \bar{\mathfrak{T}}_{G,i}(v)}{\partial \left(\frac{P_i P_{gas,G,i}}{T_i} e^{k_l T_i} \right) n} \quad (\text{C2})$$

434 $\bar{\mathfrak{T}}_{G,i}(v)$ is the layer-by-layer transmission at a 1 cm^{-1} resolution outputted from line-by-
 435 line calculation at a reference state (280K surface temperature in this study and as pro-
 436 vided in the supplementary).

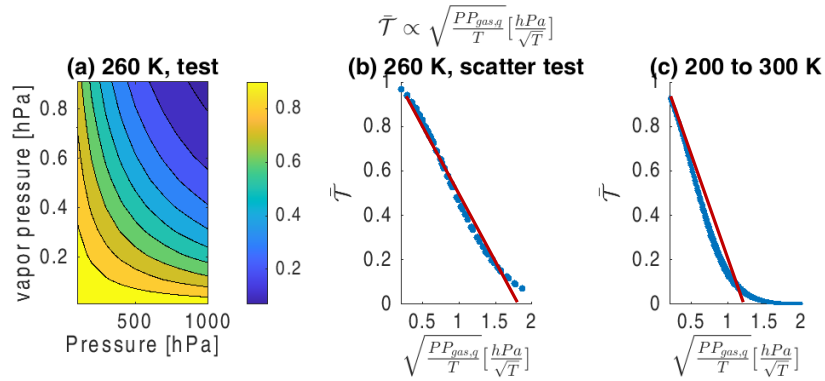


Figure C1. $\bar{\mathfrak{T}}_{G,i}(v)$ at 200 cm^{-1} is roughly proportional to $\sqrt{\frac{P P_{gas,G=q}}{T}}$, when water vapor
 is the only GHG. (a) Transmission from a test LBL run as a function of air pressure and vapor
 pressure when fixing temperature at 260 K for every 50-meter layer. (b) same as (a) but showing
 transmission as a function of $\sqrt{\frac{P P_{gas,G=q}}{T}}$ in blue dots. (c) same as (b) but from a set of real-
 istic atmospheric profiles, with temperature ranging from 200 to 300 K, for every 50-meter layer.
 Red lines in (b) and (c) are linear-approximation of two set of LBL calculations.

437 C1 Well-mixed

For well-mixed gas with constant volumn-mixing ratio n , $P_{gas,i} \equiv n P_i$. If surface
 warms from T_s to T'_s , $\bar{\mathfrak{T}}_{G,i}(v)$ in Eq. C1 can be reached at T'_i , when $k_l = 0$:

$$\begin{aligned} \bar{\mathfrak{T}}_{G,i}(T_i, v) &= \bar{\mathfrak{T}}_{G,i}(T'_i, v) \\ \frac{P_i^2}{T_i} &= \frac{P_i^2}{T_i'} \left[\frac{T_s}{T_s'} \right]^{2A(\Gamma_e)} \left[\frac{T'_i}{T_i} \right]^{2A(\Gamma)} \\ r &= \frac{T'_i}{T_i} = \frac{T_s'}{T_s} \frac{2A(\Gamma_e)}{2A(\Gamma) + k_l - 1} \end{aligned} \quad (\text{C3})$$

438 The RHS is a function of T_s . Hence, the air temperature that contributes the same weight
 439 to TOA systematically increases by r .

440 This approximation of $k_l = 0$ holds well for CH₄, N₂O, and tropospheric O₃, due
 441 to their low concentration in Earth atmosphere. The coefficient for temperature-dependent
 442 line intensity, k_l , is taken to be 0.02 for CO₂. For CO₂-only atmosphere, r is approxi-
 443 mated to:

$$r \approx \frac{\frac{2A(\Gamma)-1}{T_s} + k_l}{\frac{2A(\Gamma)-1}{T'_s} + k_l} + \frac{A(\Gamma_e) - A(\Gamma)}{T_i F'} \ln \frac{T'_s}{T_s} \quad (\text{C4})$$

444 C2 Water Vapor

The partial pressure of water vapor P_q , unlike well-mixed gases, is determined by saturation vapor pressure and relative humidity. $\bar{\mathfrak{T}}_{ql,i}(v)$ due to line absorption of water vapor is:

$$\begin{aligned} \bar{\mathfrak{T}}_{ql,i}(v) &\approx 1 - \bar{k}_{ql}(v) \left[\frac{P_i P_{q,i}}{T_i} \right]^n \\ &\approx 1 - \bar{k}_{ql}(v) \left[\frac{P_i \mathcal{R} \mathcal{H}' \frac{T'_s}{T_i} A(\Gamma) \frac{T_s}{T'_s} A(\Gamma_e) e^{\bar{k}_{CC} T'_i}}{T'_i} \right]^n \end{aligned} \quad (\text{C5})$$

$$\text{where } \bar{k}_{ql} = \frac{\partial \bar{\mathfrak{T}}_{ql,i}(v)}{\left(\frac{P_i P_{q,i}}{T_i} \right)^n}$$

445 the subscript ql denotes water vapor line absorption. k_{CC} is a linear coefficient to ap-
 446 proximate the Clausius–Clapeyron equation.

447 We can solve for the r required to reach the same transmission by taking a loga-
 448 rithm of Eq. B7 and applying a first-order Taylor expansion:

$$\begin{aligned} &[A(\Gamma) - 1] \ln T_i + k_{CC} T_i - A(\Gamma_e) \ln T_s + \ln \frac{RH}{RH'} \\ &= [A(\Gamma) - 1] \ln T'_i + k_{CC} T'_i - A(\Gamma_e) \ln T'_s \\ r &\approx \frac{\ln \frac{\mathcal{R} \mathcal{H}}{\mathcal{R} \mathcal{H}'} + \ln \frac{T'_s}{T_s} [A(\Gamma_e) - A(\Gamma) + 1]}{T_i \left[\frac{A-1}{T'_s} + k_{CC} \right]} + \frac{\frac{A-1}{T_s} + k_{CC}}{\frac{A-1}{T'_s} + k_{CC}} \end{aligned} \quad (\text{C6})$$

Self-continuum absorption of water vapor depends only on temperature that determines the vapor pressure (Paynter & Ramaswamy, 2011). Although the strong-line approximation does not strictly work for self-continuum absorption, a similar approximation can be applied to account for the impact of vapor pressure on the averaged transmission between $v - \delta v/2$ and $v + \delta v/2$ due to self-continuum absorption:

$$\begin{aligned} \bar{\mathfrak{T}}_{qc,i}(v) &\approx 1 - \bar{k}_{qc}(v) \left[\frac{P_{q,i}^2}{T_i} \right]^n \\ &\approx 1 - \bar{k}_{qc}(v) \left(\frac{\mathcal{R} \mathcal{H}^2 e^{2k_{CC} T_i}}{T_i} \right)^n \end{aligned} \quad (\text{C7})$$

$$\text{where } \bar{k}_{qc} = \frac{\partial \bar{\mathfrak{T}}_{qc,i}(v)}{\partial \left(\frac{P_{q,i}^2}{T_i} \right)^n}$$

449 with the subscript qc denotes water vapor self-continuum absorption. This approxima-
 450 tion neglects the effect of temperature on continuum absorption, partly leads to bias in
 451 Figure 3 at high surface temperature.

452

C3 Overlap

A log of averaged transmittance between $v - \delta v/2$ and $v + \delta v/2$ is taken:

$$\ln \bar{\mathfrak{T}}_i(v) = \ln \prod_G \bar{\mathfrak{T}}_{G,i}(v) + \ln \bar{\mathfrak{T}}_{ql,i}(v) + \ln \bar{\mathfrak{T}}_{qc,i}(v) \quad (\text{C8})$$

453

454

where G denotes for greenhouse gases other than water vapor, including CO_2 , CH_4 , N_2O , and O_3 .

455

456

By taking a first-order approximation of the logarithm of this equation, we can solve for r as:

$$r \approx \frac{\frac{F_1}{T_s} + F_2}{\frac{F_1}{T_s'} + F_2} + \frac{1}{T_i(\frac{F_1}{T_s'} + F_2)} \left\{ f_{CC} \ln \frac{\mathcal{RH}}{\mathcal{RH}'} + f_{BM} [A(\Gamma_e) - A(\Gamma)] \ln \frac{T_s'}{T_s} \right\} \quad (\text{C9})$$

$$\text{where } F_1 = f_{BM} A - f_{\text{Sum}}$$

$$F_2 = f_{CC} k_{CC} + f_{\text{CO}_2} k_l$$

457

458

459

460

461

462

463

Here f_{CC} represents the response from exponential dependence of saturation vapor pressure on air temperature, f_{BM} represents the response from foreign pressure that is regulated by lapse rate under the hydrostatic balance, f_{Sum} represents the response from the effect of temperature in mass density. The dependence of line intensity of CO_2 on temperature is included using $k_l = 0.02$. These coefficients can be estimated from radiative transfer calculations performed at the base state, by treating \bar{k}_{wghg} , \bar{k}_{ql} and \bar{k}_{qc} as regression coefficients and adopting $n = 0.5$:

$$\begin{cases} f_{CC} &= 2f_{qc} + f_{ql} \\ f_{BM} &= 2f_G + f_{ql} \\ f_{\text{Sum}} &= f_{\text{wghg}} + f_{ql} + f_{qc} \end{cases}$$

where :

$$\begin{cases} f_{qc} &= \frac{\bar{k}_{qc}(v) P_q^2}{\bar{k}_{qc}(v) P_q^2 + 1} \\ f_{ql} &= \frac{\bar{k}_{ql}(v) P_q}{\bar{k}_{ql}(v) P_q + 1} \\ f_{\text{wghg}} &= \frac{\sum_G \bar{k}_G(v)}{\sum_G \bar{k}_G(v) + 1}, G = \text{CO}_2, \text{CH}_4, \text{N}_2\text{O}, \text{and } \text{O}_3 \\ f_{\text{CO}_2} &= \frac{\bar{k}_{\text{CO}_2}(v)}{\bar{k}_{\text{CO}_2}(v) + 1} \end{cases} \quad (\text{C10})$$

464

465

466

467

468

469

These coefficients are estimated at every wavenumber. The same technique applies to broadband approximation (being tested for 10 cm^{-1} and for the entire infrared from 20 to 3250 cm^{-1}). Note here coefficients of O_3 are treated as well-mixed gases because tropospheric O_3 does not strongly vary with height (or air temperature). Figure .C2 shows the predicted feedback parameters with different mixtures of greenhouse gases, in comparison with LBL results which exclude changes in the stratosphere.

470

471

472

473

474

475

476

477

478

479

480

In Eq. B11 (and Eq. 4), the magnitude of r depends on the fractional contributions and the lapse rate. As f_{Sum} and k_l are small ($f_{\text{Sum}} \ll f_{BM}$ and $k_l \ll k_{CC}$), r is close to $\frac{T_s + \Delta T}{T_s}$ if the effect of pressure on transmission is more significant than the effect of vapor pressure (i.e., $f_{BM} \gg f_{CC}$), as in the case of strong absorption channels of well-mixed gases (i.e., Fig. 3(b) 500 to 800 cm^{-1} and Fig. 3(d)). In water vapor absorption channels, r is dampened by f_{CC} , hence r as inferred from Fig. 2 is less than $\frac{T_s + \Delta T}{T_s}$ but still greater than one owing to f_{BM} . On the other hand, lapse rate describes the air temperature-pressure relationship via $A(\Gamma)$ and $A(\Gamma_e)$. A large $A(\Gamma_e)$ caused by dramatic surface expansion above a warm, moist surface (small Γ_e) is associated with an amplified warming in atmosphere than the surface ($A(\Gamma_e) > A(\Gamma)$), leading to larger r and more negative feedback.

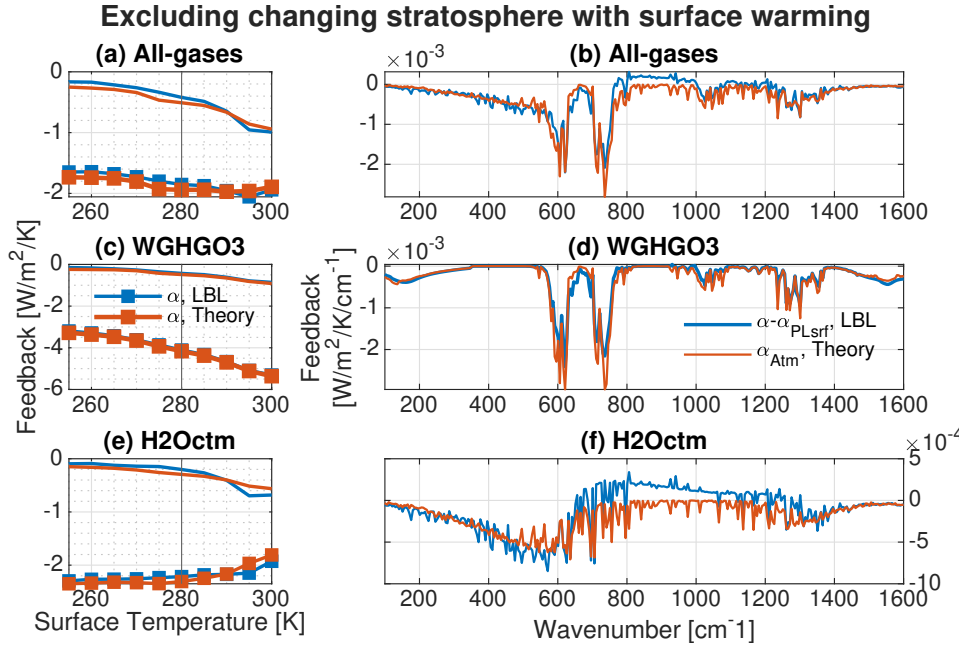


Figure C2. Similar to Fig. 3, clear-sky longwave feedback with different mixture of greenhouse gases but excluding stratospheric feedback for validating Eq. B2 and Eq. B12. Left: clear-sky longwave feedback (α , solid curve with marker) and atmospheric feedback (α_{Atm} , solid) from line-by-line calculations (blue) and from theoretical predictions (red) with different mixture of greenhouse gas: (a) all greenhouse gases (All-gases), (c) well-mixed GHGs and O_3 (WGHGO3), and (e) water vapor (H_2O). Right: similar to left panels but for spectrally decomposed atmospheric feedback ($\alpha_{\text{Atm}}(v)$) at $280 \text{ K } T_s$, convoluted from 1 cm^{-1} to 5 cm^{-1} .

481 **Acknowledgments**

482 We acknowledge GFDL resources made available for this research. Nadir Jeevanjee and
 483 Shiv Priyam Raghuraman are acknowledged for their comments and suggestions on an
 484 internal review of the manuscript.

485 **References**

486 Bourdin, S., Kluft, L., & Stevens, B. (2021). Dependence of climate sensitivity
 487 on the given distribution of relative humidity. *Geophysical Research Letters*,
 488 *48*(8), e2021GL092462.
 489 Clough, S. A., & Iacono, M. J. (1995). Line-by-line calculation of atmospheric fluxes
 490 and cooling rates: 2. application to carbon dioxide, ozone, methane, nitrous
 491 oxide and the halocarbons. *Journal of Geophysical Research: Atmospheres*,
 492 *100*(D8), 16519–16535.
 493 Donner, L. J., Wyman, B. L., Hemler, R. S., Horowitz, L. W., Ming, Y., Zhao, M.,
 494 ... others (2011). The dynamical core, physical parameterizations, and basic
 495 simulation characteristics of the atmospheric component am3 of the gfdl global
 496 coupled model cm3. *Journal of Climate*, *24*(13), 3484–3519.
 497 Feng, J., & Huang, Y. (2019). Diffusivity-factor approximation for spectral outgoing
 498 longwave radiation. *Journal of the Atmospheric Sciences*, *76*(7), 2171–2180.
 499 Goldblatt, C., Robinson, T. D., Zahnle, K. J., & Crisp, D. (2013). Low simulated
 500 radiation limit for runaway greenhouse climates. *Nature Geoscience*, *6*(8), 661–
 501 667.

- 502 Goody, R., & Yung, Y. (1989). *Atmospheric radiation, 519 pp.* Oxford Univ. Press,
503 New York.
- 504 Griffies, S. M., Winton, M., Donner, L. J., Horowitz, L. W., Downes, S. M., Farneti,
505 R., . . . others (2011). The gfdl cm3 coupled climate model: characteristics of
506 the ocean and sea ice simulations. *Journal of Climate*, *24*(13), 3520–3544.
- 507 Held, I. M., & Shell, K. M. (2012). Using relative humidity as a state variable in cli-
508 mate feedback analysis. *Journal of Climate*, *25*(8), 2578–2582.
- 509 Huang, Y., & Bani Shahabadi, M. (2014). Why logarithmic? a note on the de-
510 pendence of radiative forcing on gas concentration. *Journal of Geophysical Re-*
511 *search: Atmospheres*, *119*(24), 13–683.
- 512 Ingersoll, A. P. (1969). The runaway greenhouse: A history of water on venus. *Jour-*
513 *nal of Atmospheric Sciences*, *26*(6), 1191–1198.
- 514 Ingram, W. (2010). A very simple model for the water vapour feedback on climate
515 change. *Quarterly Journal of the Royal Meteorological Society: A journal*
516 *of the atmospheric sciences, applied meteorology and physical oceanography*,
517 *136*(646), 30–40.
- 518 Ingram, W. (2013). A new way of quantifying gcm water vapour feedback. *Climate*
519 *dynamics*, *40*(3), 913–924.
- 520 Jeevanjee, N., Koll, D. D., & Lutsko, N. (2021). “simpson’s law” and the spec-
521 tral cancellation of climate feedbacks. *Geophysical Research Letters*, *48*(14),
522 e2021GL093699.
- 523 Kluft, L., Dacie, S., Brath, M., Buehler, S. A., & Stevens, B. (2021). Temperature-
524 dependence of the clear-sky feedback in radiative-convective equilibrium. *Geo-*
525 *physical Research Letters*, *48*(22), e2021GL094649.
- 526 Koll, D. D., & Cronin, T. W. (2018). Earth’s outgoing longwave radiation linear
527 due to h2o greenhouse effect. *Proceedings of the National Academy of Sciences*,
528 *115*(41), 10293–10298.
- 529 McKim, B. A., Jeevanjee, N., & Vallis, G. K. (2021). Joint dependence of longwave
530 feedback on surface temperature and relative humidity. *Geophysical Research*
531 *Letters*, *48*(18), e2021GL094074.
- 532 Nakajima, S., Hayashi, Y.-Y., & Abe, Y. (1992). A study on the “runaway green-
533 house effect” with a one-dimensional radiative–convective equilibrium model.
534 *Journal of Atmospheric Sciences*, *49*(23), 2256–2266.
- 535 Paynter, D., Frölicher, T., Horowitz, L., & Silvers, L. (2018). Equilibrium climate
536 sensitivity obtained from multimillennial runs of two gfdl climate models.
537 *Journal of Geophysical Research: Atmospheres*, *123*(4), 1921–1941.
- 538 Paynter, D., & Ramaswamy, V. (2011). An assessment of recent water vapor con-
539 tinuum measurements upon longwave and shortwave radiative transfer. *Jour-*
540 *nal of Geophysical Research: Atmospheres*, *116*(D20).
- 541 Pierrehumbert, R. T. (2010). *Principles of planetary climate.* Cambridge University
542 Press.
- 543 Raghuraman, S. P., Paynter, D., & Ramaswamy, V. (2019). Quantifying the drivers
544 of the clear sky greenhouse effect, 2000–2016. *Journal of Geophysical Research:*
545 *Atmospheres*, *124*(21), 11354–11371.
- 546 Seeley, J. T., & Jeevanjee, N. (2021). H2o windows and co2 radiator fins: A clear-
547 sky explanation for the peak in equilibrium climate sensitivity. *Geophysical Re-*
548 *search Letters*, *48*(4), e2020GL089609.
- 549 Sherwood, S., Webb, M. J., Annan, J. D., Armour, K. C., Forster, P. M., Harg-
550 reaves, J. C., . . . others (2020). An assessment of earth’s climate sensitivity us-
551 ing multiple lines of evidence. *Reviews of Geophysics*, *58*(4), e2019RG000678.
- 552 Simpson, S. G. C. (1928). Some studies in terrestrial radiation. *Memoirs of the royal*
553 *meteorological society*, *11*(16), 69–95.
- 554 Zelinka, M. D., Myers, T. A., McCoy, D. T., Po-Chedley, S., Caldwell, P. M., Ceppi,
555 P., . . . Taylor, K. E. (2020). Causes of higher climate sensitivity in cmip6
556 models. *Geophysical Research Letters*, *47*(1), e2019GL085782.

557 Zhang, Y., Jeevanjee, N., & Fueglistaler, S. (2020). Linearity of outgoing longwave
558 radiation: From an atmospheric column to global climate models. *Geophysical*
559 *Research Letters*, *47*(17), e2020GL089235.